Copy _____

IDA PAPER P-2978

CHARACTERIZING AND CORRECTING MEDIA-INDUCED FOCUS ERRORS IN SYNTHETIC APERTURE RADAR IMAGERY

Gerald Gilbert
Matthew Braunstein
James Ralston

April 1994

Prepared for
Information Systems Office – ARPA

INSTITUTE FOR DEFENSE ANALYSES
1801 N. Beauregard Street, Alexandria, Virginia 22311-1772

IDA Log No. H 94-45672

DEFINITIONS

IDA publishes the following documents to report the results of its work.

Reports

Reports are the most authoritative and most carefully considered products IDA publishes. They normally embody results of major projects which (a) have a direct bearing on decisions affecting major programs, (b) address issues of significant concern to the Executive Branch, the Congress and/or the public, or (c) address issues that have significant economic implications. IDA Reports are reviewed by outside panels of experts to ensure their high quality and relevance to the problems studied, and they are released by the President of IDA.

Group Reports

Group Reports record the findings and results of IDA established working groups and panels composed of senior individuals addressing major issues which otherwise would be the subject of an IDA Report. IDA Group Reports are reviewed by the senior individuals responsible for the project and others as selected by IDA to ensure their high quality and relevance to the problems studied, and are released by the President of IDA.

Papers

Papers, also authoritative and carefully considered products of IDA, address studies that are narrower in scope than those covered in Reports. IDA Papers are reviewed to ensure that they meet the high standards expected of refereed papers in professional journals or formal Agency reports.

Documents

IDA Documents are used for the convenience of the sponsors or the analysts (a) to record substantive work done in quick reaction studies, (b) to record the proceedings of conferences and meetings, (c) to make available preliminary and tentative results of analyses, (d) to record data developed in the course of an investigation, or (e) to forward information that is essentially unanalyzed and unevaluated. The review of IDA Documents is suited to their content and intended use.

The work reported in this document was conducted under contract DASW01 94 C 0054 for the Department of Defense. The publication of this IDA document does not indicate endorsement by the Department of Defense, nor should the contents be construed as reflecting the official position of that Agency.

IDA PAPER P-2978

CHARACTERIZING AND CORRECTING MEDIA-INDUCED FOCUS ERRORS IN SYNTHETIC APERTURE RADAR IMAGERY

Gerald Gilbert
Matthew Braunstein
James Ralston

April 1994

INSTITUTE FOR DEFENSE ANALYSES
Contract DASW01 94 C 0054
ARPA Assignment A-155

PREFACE

This paper was prepared by the Institute for Defense Analyses for the Advanced Projects Research Agency under a task entitled "Ultra-Wideband Radar Technology Evaluation."

This paper was reviewed by IDA staff members Dr. Arthur Krinitz and Dr. Roger Sullivan.

This work represents a contribution to the ongoing effort directed toward the improvement of our understanding of the applications of ultra-wideband radar.

CONTENTS

FIGURES

(n.b.: In the figures we have defined – $z \equiv z'$.)

SUMMARY

This paper examines an important basic issue which underlies the construction of algorithms used in synthetic aperture radar (SAR) image reconstruction; in particular, SAR image reconstruction in the context of ground-penetrating radar (GPR) applications. It is currently the case that the development of GPR image reconstruction algorithms is often based on assumptions developed in the context of free-space radar propagation to the reconstruction of images of buried objects from the SAR data [1,2]. Although in many cases the assumption of free-space propagation leads to results which are acceptable; in some important cases it will result in severe degradation to radar images of underground objects. We conclude that the assumption of plane wave radar propagation gives rise to poorer image quality as the SAR receiving antenna is brought into closer proximity with the air-ground interface. This degradation occurs because as the interface is approached, a surface wave component of the total electromagnetic field known as the *lateral wave* becomes a significant factor in determining target signal history and radar response, and this component is entirely absent in the plane wave approximation. Improvements in image quality do result upon modifying the assumption of free-space plane wave propagation by incorporating the effects of refraction on plane waves. However, additional improvements in focusing quality result upon completely replacing the plane wave model with the explicit solution dictated by the actual boundary conditions appropriate to GPR problems. Then the electromagnetic field necessarily includes the lateral wave, the analytical form of which is incompatible with any plane wave [3]. We are therefore led to propose that, in certain specific circumstances, the current reliance on plane waves as putative radar waveforms in SAR image reconstruction should be abandoned in favor or more accurate solutions to the Maxwell equations.

1. INTRODUCTION

In this paper we shall examine an important basic issue which underlies the construction of algorithms used in synthetic aperture radar (SAR) image reconstruction. In particular we will be concerned with SAR image reconstruction in the context of ground-penetrating radar (GPR) applications. We will study the extent to which one may apply assumptions developed in the context of free-space radar propagation to the reconstruction of images of buried objects from SAR data. It is currently the case that the development of GPR image reconstruction algorithms is often based on such assumptions [1, 2].

2. ANALYSIS

We shall consider the effect on SAR image reconstruction of the specific waveforms assumed to model the actual electromagnetic radiation in practical GPR problems. We shall take the overall geometry to be modeled by two semi-infinite half-spaces ("air" and "ground," respectively) separated by a planar interface. We shall employ at our convenience both cylindrical (ρ, ϕ, z) and rectilinear (x, y, z) coordinate systems such that in each case the z-coordinate increases in value in the *downward* direction. The ground will be modeled as a lossy, electrically homogeneous and isotropic, non-magnetic medium. The region above the interface (air) will be referred to as region 2, and the region below the interface (ground) will be referred to as region 1. The corresponding wavenumbers will be designated as k_2 ($\in \mathbf{R}$) and k_1 ($\in \mathbf{C}$), respectively. We will consider a side-looking SAR receiving antenna moving at a fixed altitude $|z|$ and displaced a fixed distance y from a buried dipole located at cylindrical (and rectilinear) coordinates $(0,0,d)$ (see Figure 1).[1] It will prove useful to define the quantities r_0, r_d, and r_2 as

$$r_0 = \sqrt{\rho^2 + z^2} \quad , \tag{1a}$$

$$r_d = \sqrt{\rho^2 + d^2} \quad , \tag{1b}$$

$$r_2 = \sqrt{\rho^2 + (z+d)^2} \quad . \tag{1c}$$

We will also need the function $F(x) = \frac{1}{2}(1+i) - C_2(x) - iS_2(x)$, where $C_2(x) + iS_2(x)$ denotes the Fresnel integral of the second kind as a function of x, and

$$P = p_1 \left(\frac{p_1 - p_2}{p_3} \right)^2 \tag{1d}$$

with $p_1 = \dfrac{k_2^3 r_2}{2k_1^2}$, $p_2 = \dfrac{k_2^2 z}{2k_1}$, and $p_3 = \dfrac{k_2^3 \rho}{2k_1^2}$ for $z \le 0$.

---

[1] The analysis presented here is for the one-way specialization of the complete radar problem comprising a buried source and an elevated receiver. This allows direct application of prior work on electromagnetic propagation and can be extended to the complete two-way radar propagation case [4].

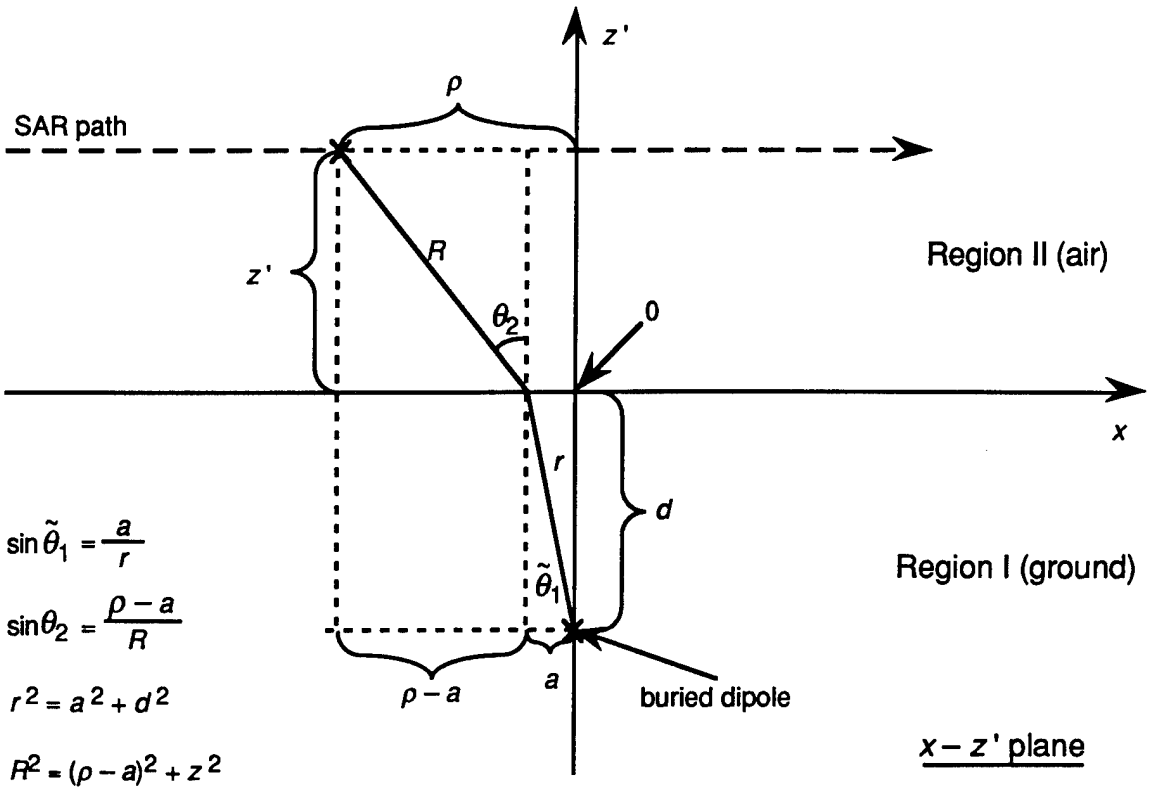

Figure 1. GPR Geometry

We will take the source of the electromagnetic field to be a buried horizontal (x-directed) infinitesimal point dipole with dipole moment normalized to unity. The complete solution to the Maxwell equations in region 2 (i.e., $z \le 0$) for an infinitesimal horizontal dipole with unit moment buried at a depth d in region 1 has been worked out by King and Wu [5] and is given by

$$E_\rho^{\mathrm{KW}}(\rho,\phi,z) = -\frac{\omega\mu_0}{2\pi k_1^2}\cos\phi$$

$$\times\left(e^{ik_1 d} e^{ik_2 r_0}\left\{ k_2\left[\frac{ik_2}{r_0} - \frac{1}{r_0^2} - \frac{i}{k_2 r_0^3} - \frac{k_2^3}{k_1}\left(\frac{r_2}{\rho}\right)\left(\frac{\pi}{k_2 r_2}\right)^{1/2} e^{-iP} F(P)\right]\right.\right.$$

$$\left.\left. + k_1\left(\frac{z}{r_0}\right)\left(\frac{ik_2}{r_0} - \frac{1}{r_0^2}\right)\right\}\right.$$

$$- e^{k_1 z} e^{ik_1 r_d} k_1\left[\frac{1}{r_d^2} + \frac{i}{k_1 r_d^3} - \left(\frac{d}{\rho}\right)\left(\frac{i}{\rho^2} - \frac{3}{2k_1\rho^3}\right)\right.$$

$$\left.\left. + \left(\frac{d}{r_d}\right)^2\left(\frac{ik_1}{r_d} - \frac{3}{r_d^2} - \frac{3i}{k_1 r_d^3}\right)\right]\right) , \qquad (2)$$

$$E_{\phi}^{\mathrm{KW}}(\rho,\phi,z)=\frac{\omega\mu_0}{2\pi k_1^2}\sin\phi$$

$$\times\left(e^{ik_1 d}e^{ik_2 r_0}\left\{k_2\left[\frac{2}{r_0^2}+\frac{2i}{k_2 r_0^3}+\frac{ik_2^2}{k_1\rho}\left(\frac{r_2^2}{\rho^2}\right)\left(\frac{\pi}{k_2 r_2}\right)^{1/2}e^{-iP}F(P)\right.\right.\right.$$

$$\left.\left.+\left(\frac{z}{r_0}\right)^2\left(\frac{ik_2}{r_0}-\frac{3}{r_0^2}-\frac{3i}{k_2 r_0^3}\right)\right]\right.$$

$$\left.+k_1\left(\frac{z}{r_0}\right)\left(\frac{ik_2}{r_0}-\frac{1}{r_0^2}\right)\right\}$$

$$-e^{k_1 z}e^{ik_1 r_d}k_1\left[\frac{1}{r_d^2}+\frac{i}{k_1 r_d^3}-i\left(\frac{d}{r_d}\right)\left(\frac{ik_1}{\rho}-\frac{3}{2\rho^2}-\frac{5i}{8k_1\rho^3}\right)\right.$$

$$\left.\left.+\left(\frac{d}{r_d}\right)^2\left(\frac{ik_1}{r_d}-\frac{3}{r_d^2}-\frac{3i}{k_1 r_d^3}\right)\right]\right)\quad , \tag{3}$$

$$E_z^{\mathrm{KW}}(\rho,\phi,z)=\frac{\omega\mu_0}{2\pi k_1}\cos\phi\left\{e^{ik_1 d}e^{ik_2 r_0}\left[\left(\frac{\rho}{r_0}\right)\left(\frac{ik_2}{r_0}-\frac{1}{r_0^2}\right)-\frac{k_2^3}{k_1}\left(\frac{\pi}{k_2 r_2}\right)^{1/2}e^{-iP}F(P)\right]\right.$$

$$\left.-e^{k_1 z}e^{ik_1 r_d}\left(\frac{i}{\rho^2}-\frac{3}{2k_1\rho^3}\right)\right\}\quad . \tag{4}$$

Here ω is the circular frequency and μ_0 is the magnetic permeability of free-space. The above solution is valid *everywhere* in region 2, subject only to the restriction $|k_1|\geq 3|k_2|$.[2,3]

In the subsequent analysis it will be useful for us to define the component in the direction of motion of the SAR receiving antenna of the above solution as the function

$$f_1(\mathbf{x})\equiv E_x^{\mathrm{KW}}(\mathbf{x})\quad . \tag{5}$$

---

2 Note that the expression given for $E_z^{\mathrm{KW}}(\rho,\phi,z)$ in Eq. (4) above differs from the expression given in Eq. (5.10.1b) on p. 221 of [5]. There is an incorrect factor of r_2/ρ multiplying *F(P)* in Eq. (5.10.1b) of [5] *when applied to* E_z [6], which should be replaced by unity, and this is done in Eq. (4) above.

3 The inequality $|k_1|\geq 3|k_2|$ is a consequence of the assumption that the wavenumbers k_1 and k_2 are significantly different from each other, or that $|k_1|^2 >> |k_2|^2$.

We are interested in isolating and illustrating the effect on focusing quality which results from successively improving upon the free-space plane wave model by first taking into account refraction effects in plane waves and then making use instead of the full King-Wu solution. In assessing the consequences of different choices of radar waveforms in SAR image reconstruction we shall thus introduce additional functions chosen to illustrate the successive improvement in focusing quality:

$$f_2(\mathbf{x}) \equiv E^{ik_2 r_2(|z|)}\cos\phi \tag{6}$$

[where $r_2(z)$ is given in Eq. (1c)], which is a plane wave in an infinite lossless medium, and

$$f_3(\mathbf{x}) \equiv T(\theta_1,\theta_2)e^{i(k_1 r + k_2 R)}\cos\phi \quad , \tag{7}$$

a refracted plane wave passing through lossy *and* lossless media in which refraction effects and transmission effects at the surface are accounted for through the appropriate refractive path length and through the transmission coefficient

$$T(\theta_1,\theta_2) = \frac{2k_2\cos\theta_2}{k_1\cos\theta_1 + k_2\cos\theta_2} \quad . \tag{8}$$

In the above expressions

$$R = \sqrt{(\rho - a)^2 + z^2} \quad , \tag{9a}$$

$$r = \sqrt{a^2 + d^2} \quad , \tag{9b}$$

and the transmission angles θ_1 and θ_2 are given by

$$\theta_1 = \sin^{-1}\left(\frac{k_2}{k_1}\sin\theta_2\right) \quad , \tag{10a}$$

and

$$\theta_2 = \sin^{-1}\left(\frac{\rho - a}{R}\right) \quad , \tag{10b}$$

where a satisfies the transcendental equation (derived in the appendix)

$$q^2(a)a^4 - 2\rho q^2(a)a^3 + \left[q^2(a)\left(\rho^2 + z^2\right) - k_2^2 d^2\right]a^2 + 2\rho k_2^2 d^2 a - k_2^2 d^2 \rho^2 = 0 \quad , \tag{11}$$

with

$$q(a) = |u|\left[\mathrm{Re}k_1 \cdot \cos(\arg u) - \mathrm{Im}k_1 \cdot \sin(\arg u)\right] \quad . \tag{12}$$

The quantity u which appears in Eq. (12) is the complex function of a given in Eq. (A4) of the appendix. The solution of Eq. (11), a, is the horizontal *offset distance* separating the

origin of coordinates from that point at which, in the geometrical optics approximation, the refracted ray from source to receiver impinges on the air-ground interface. Although Eq. (11) is very interesting to study and appears to have been derived here for the first time in the literature,[4] we will content ourselves with making use of numerical solutions for the purposes of the present analysis.

Comparing the King-Wu field given in Eq. (5) with the different plane wave approximations given in Eqs. (6) and (7), one may note an important distinction: the King-Wu solution includes a surface wave component known as the *lateral wave*, which is entirely absent from either of the plane waves. The characteristic features of the lateral wave are (1) the *algebraic*, rather than exponential, decay as a function of the radial coordinate ρ as the field propagates along the air-ground interface away from the buried dipole and (2) a decrease in field strength as $|z|$ increases in value. Inspection of Eqs. (2) through (4) reveals that near the interface the lateral wave becomes an important component of the total electromagnetic field. It is therefore to be expected that, as long as the SAR receiving antenna is not too high, the lateral wave component of the King-Wu solution will play an important role in determining propagation effects and therefore in determining radar response as well. These propagation effects will be markedly different from those associated with plane waves. Although it is the case that the electromagnetic field due to a point dipole in an infinite medium reduces in the limit of infinite separation from the source to an infinite plane wave, such a plane wave can never by itself include the lateral wave [3]. One is naturally led to inquire as to the extent to which such differences will manifest themselves in the quality of images constructed on the assumption of plane wave propagation.

We will therefore study the following functions to assess the image quality associated with the different choices of radar waveform listed in Eqs. (5) through (7):

$$\mu_i(\mathbf{x}) \equiv |f_1(\mathbf{x})| - |f_i(\mathbf{x})| \quad , \tag{13}$$

$$\Delta_i(\mathbf{x}) \equiv \left\{ \arg[f_1(\mathbf{x})] - \arg[f_i(\mathbf{x})] \right\}_{\text{phase-unwrapped}} \tag{14}$$

---

4 In most treatments of plane waves incident on plane boundaries (see, e.g., [7]) the point at which (in the geometrical optics approximation) the geometrical optics ray passes from one medium to the other is taken to coincide with the origin of coordinates. In our case this point is in general necessarily a function of time dependent on the moving location of the SAR antenna, and must be determined accordingly. Inspection of Figure 1 shows that the offset distance a is determined by the real, "geographical" transmission angle $\tilde{\theta}_1$ rather than the complex, "formal" transmission angle θ_1. The relation between the two transmssion angles is discussed in the appendix.

and

$$\chi_j(\mathbf{x}) \equiv \int d^3x'\, f_1(\mathbf{x}') f_j(\mathbf{x}'+\mathbf{x})^* \quad , \tag{15}$$

where $i,j = 1...3$. The two nonvanishing functions $\mu_i(\mathbf{x})$ and the two nonvanishing functions $\Delta_i(\mathbf{x})$ are the magnitude and phase differences, respectively, between the plane wave approximations and the King-Wu solution. In evaluating $\Delta_i(\mathbf{x})$ in Eq. (14), note that the quantity inside the curly brackets has been point-wise adjusted by an appropriate multiple of 2π to obtain the "phase-unwrapped" value of the function. The three correlation functions $\chi_j(\mathbf{x})$ in Eq. (15) (one auto-correlation function and two cross-correlation functions) are the zero-doppler cuts of the various one-way radar ambiguity functions [8] for the different possible waveforms.

3. NUMERICAL COMPUTATIONS

We shall numerically study the functions μ_i, Δ_i, and χ_j for four distinct, representative GPR scenarios. If we denote the linear frequency by f, these scenarios are:

Case 1a: $f =$ 600 MHz, $y = |z| =$ 3 m

Case 1b: $f =$ 600 MHz, $y = |z| =$ 30 m

Case 2a: $f =$ 5 GHz, $y = |z| =$ 3 m

Case 2b: $f =$ 5 GHz, $y = |z| =$ 30 m.

The lower altitude scenarios are intended to model GPR applications which involve ground-based receiving platforms, while the higher altitude scenarios are intended to model GPR applications which involve airborne receiving platforms. For each scenario, we shall take for region 1 the conductivity σ_1 and the real part of the electrical permitivitty ϵ_{1r} to be given by $\sigma_1 = 0.01$ S/m and $\epsilon_{1r} = 9$, respectively, and the corresponding quantities for region 2 shall be given by the respective free-space values. As noted in Section 2, we shall ignore magnetization effects. Also, as noted in Section 2, we shall consider a one-way specialization of the complete radar problem by taking the total electromagnetic field to be given by the electromagnetic waves emanating from a buried dipole target; for all four scenarios we shall take the dipole to be buried at a depth $d = 0.5$ m. For both frequencies at each altitude, graphs of the various functions were computed over a synthetic aperture of size comparable to the altitude. In all four cases the data are plotted over a cross-range "window" which is smaller than the actual synthetic aperture: of 10 m width and 3 m width, for 3 m altitude data at 600 MHz and 5 GHz, respectively, and of 20 m width and 10 m width for 30 m altitude data at 600 MHz and 5 GHz, respectively. The plots are shown in Figures 2 through 13; their implications are discussed in the following section.

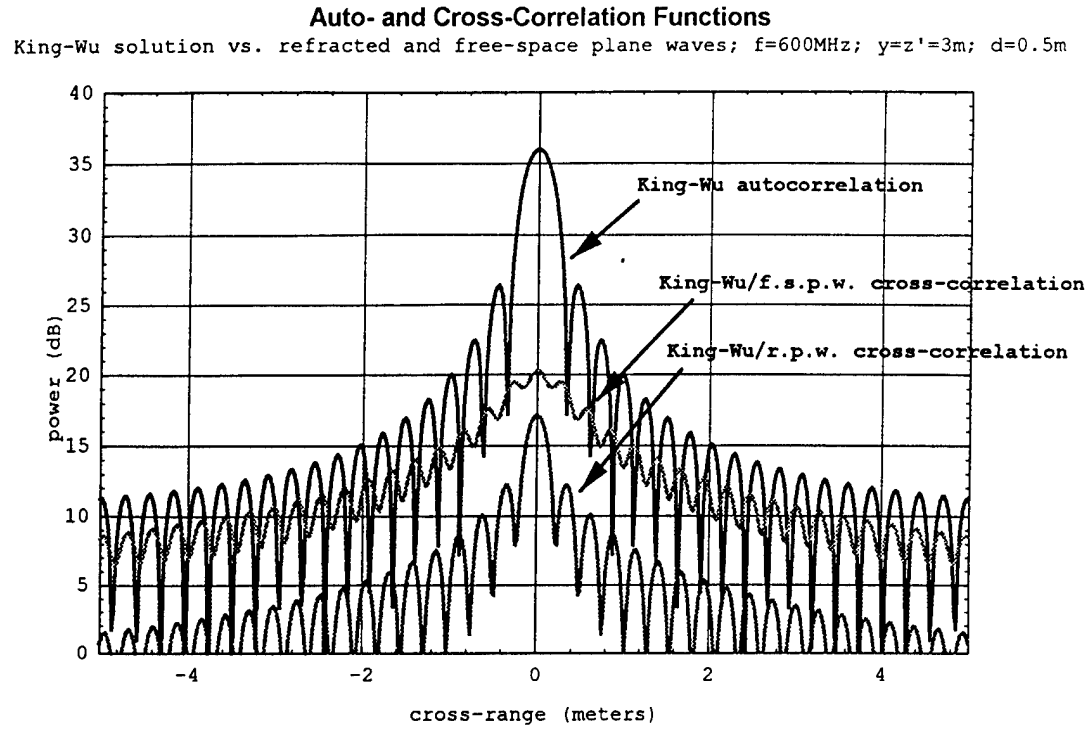

Figure 2. Correlation Functions; $|z|$ = 3 m; f = 600 MHz

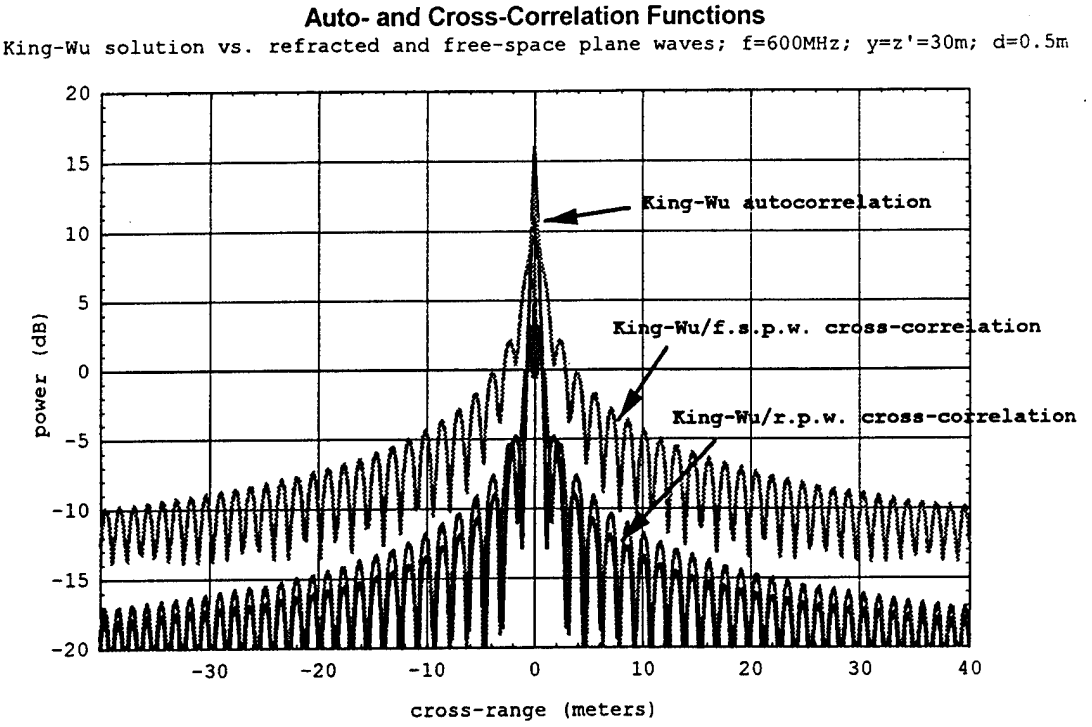

Figure 3. Correlation Functions; $|z|$ = 30 m; f = 600 MHz

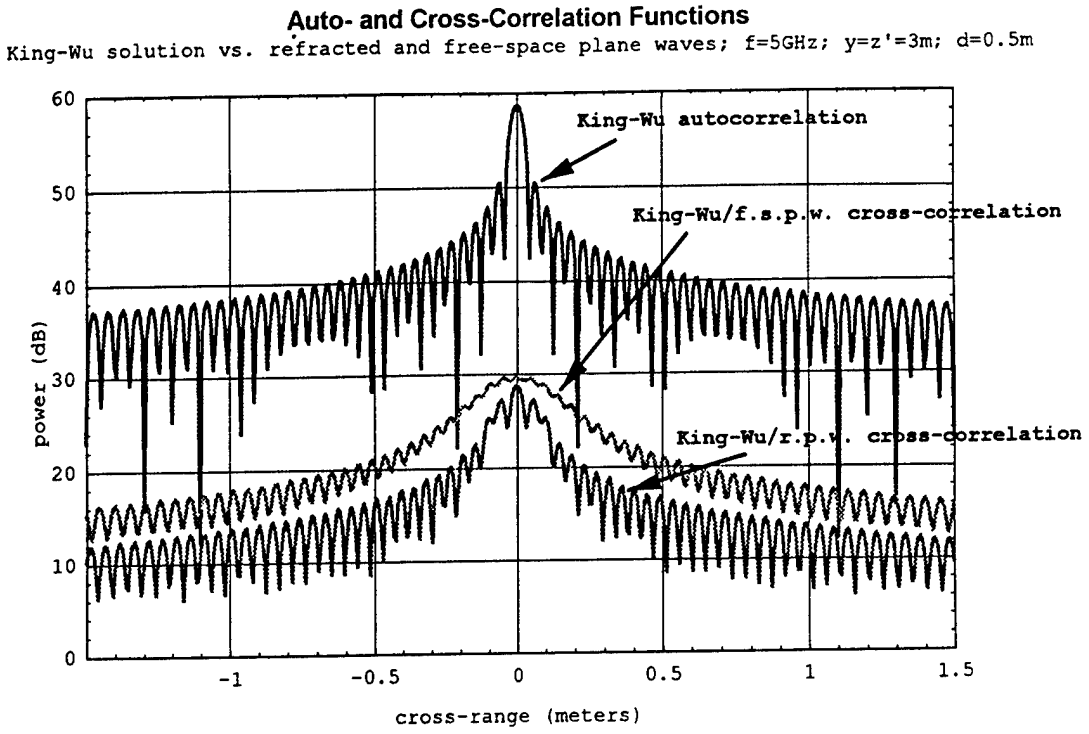

Figure 4. Correlation Functions; $|z|$ = 3 m; f = 5 GHz

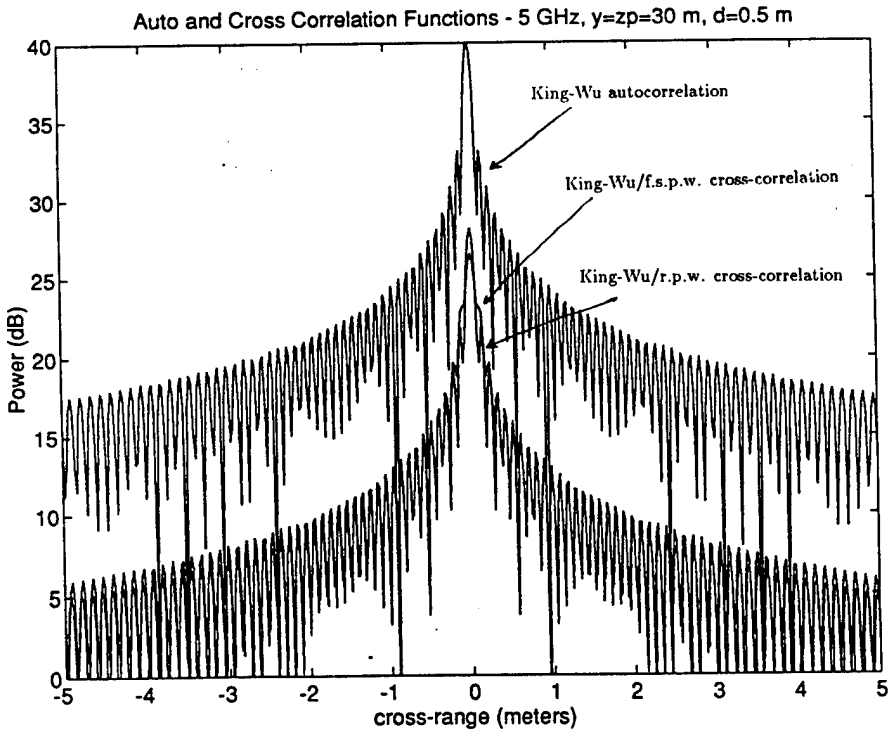

Figure 5. Correlation Functions; $|z|$ = 30 m; f = 5 GHz

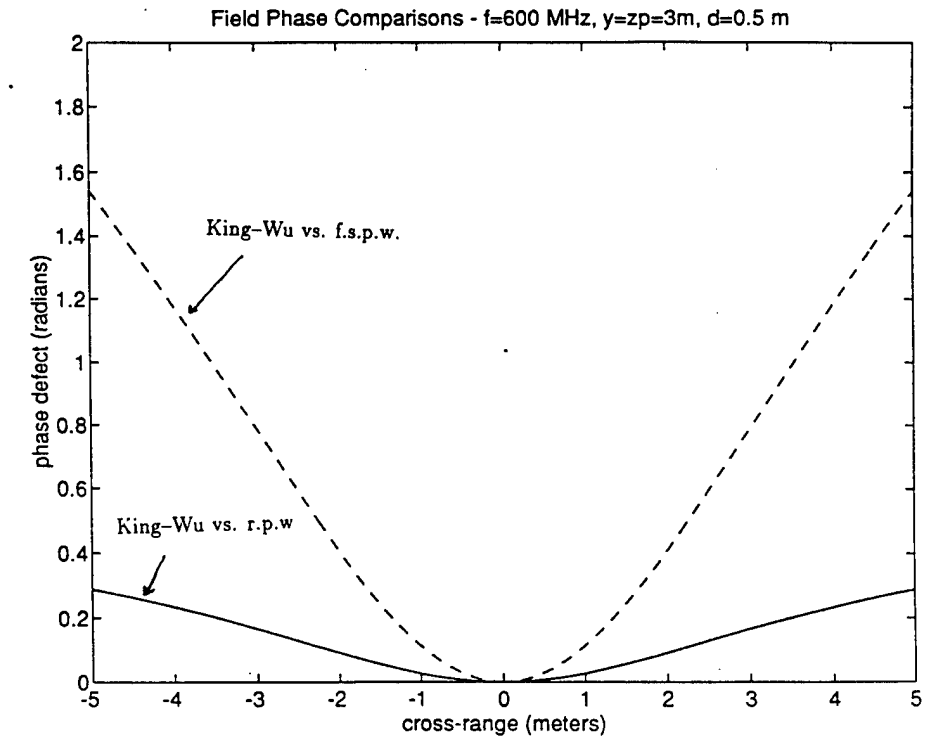

Figure 6. Field Phase Differences; $|z|$ = 3 m; f = 600 MHz

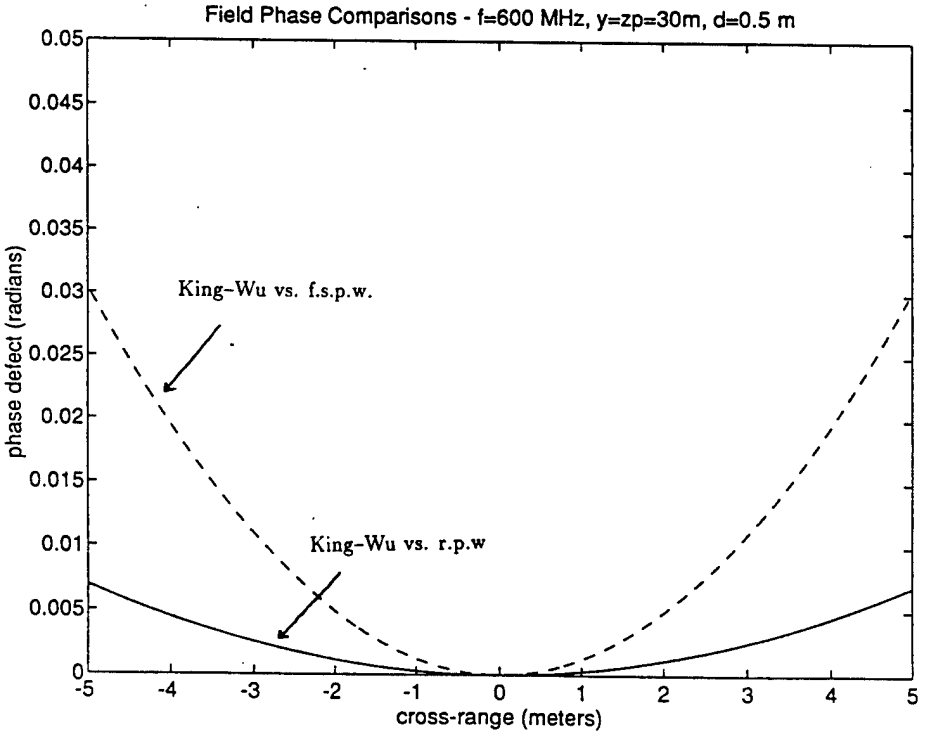

Figure 7. Field Phase Differences; $|z|$ = 30 m; f = 600 MHz

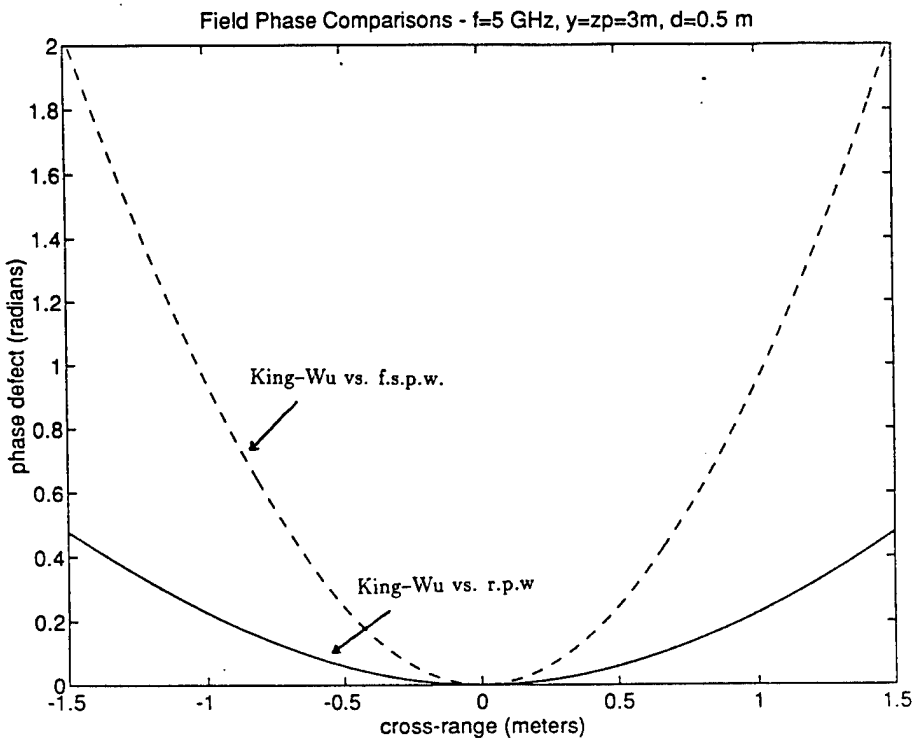

Figure 8. Field Phase Differences; $|z|$ = 3 m; f = 5 GHz

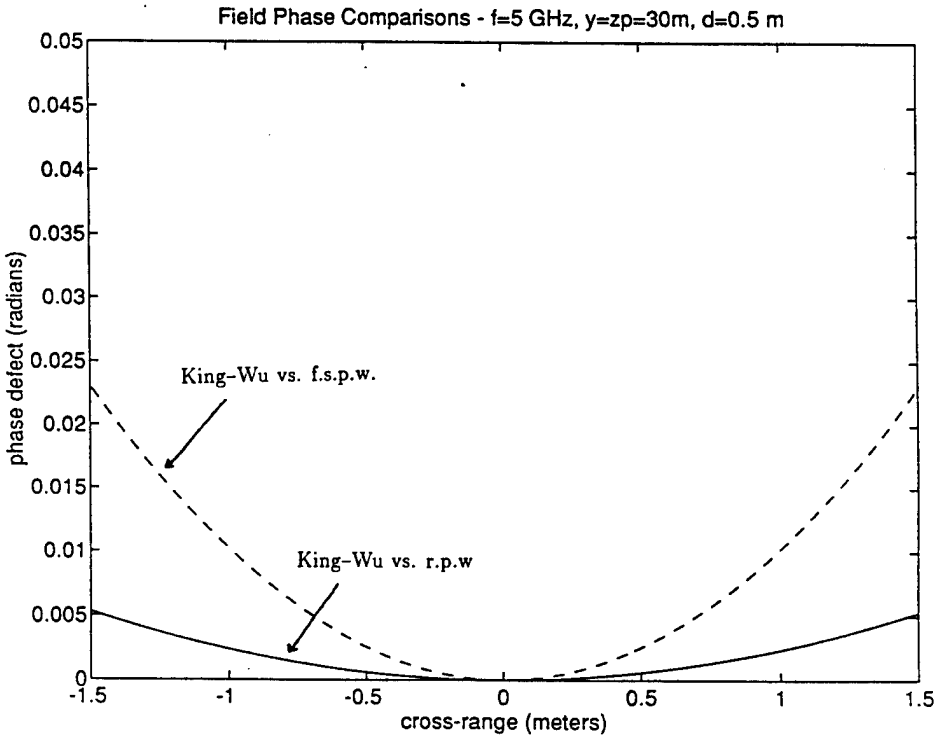

Figure 9. Field Phase Differences; $|z|$ = 30 m; f = 5 GHz

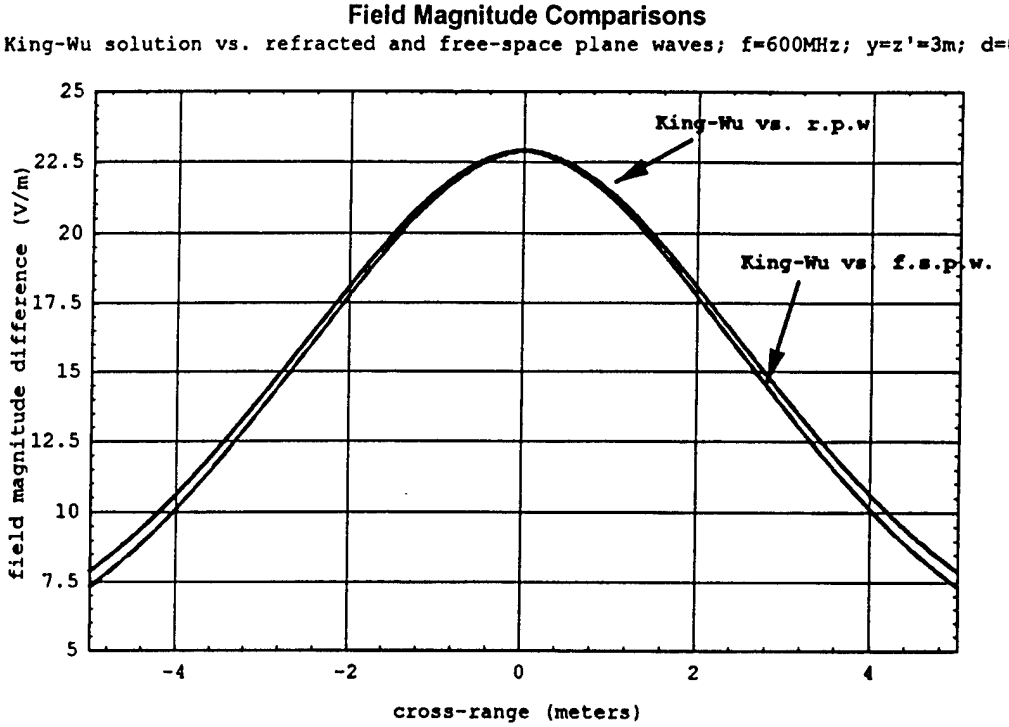

Figure 10. Field Magnitude Differences; $|z|$ = 3 m; f = 600 MHz

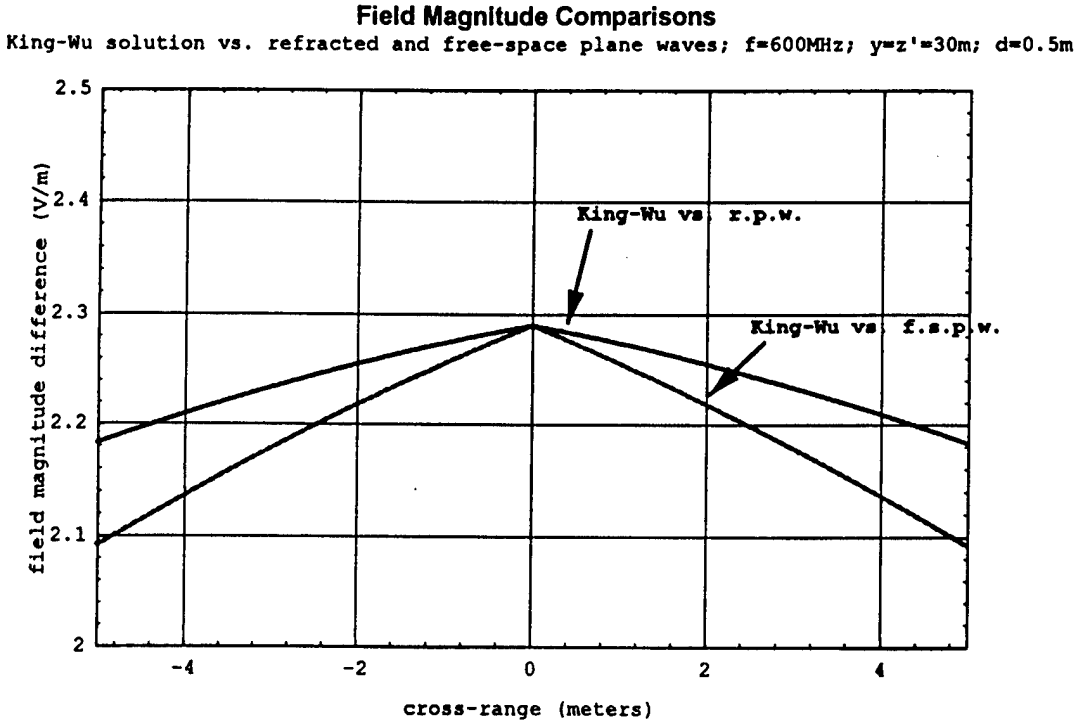

Figure 11. Field Magnitude Differences; $|z|$ = 30 m; f = 600 MHz

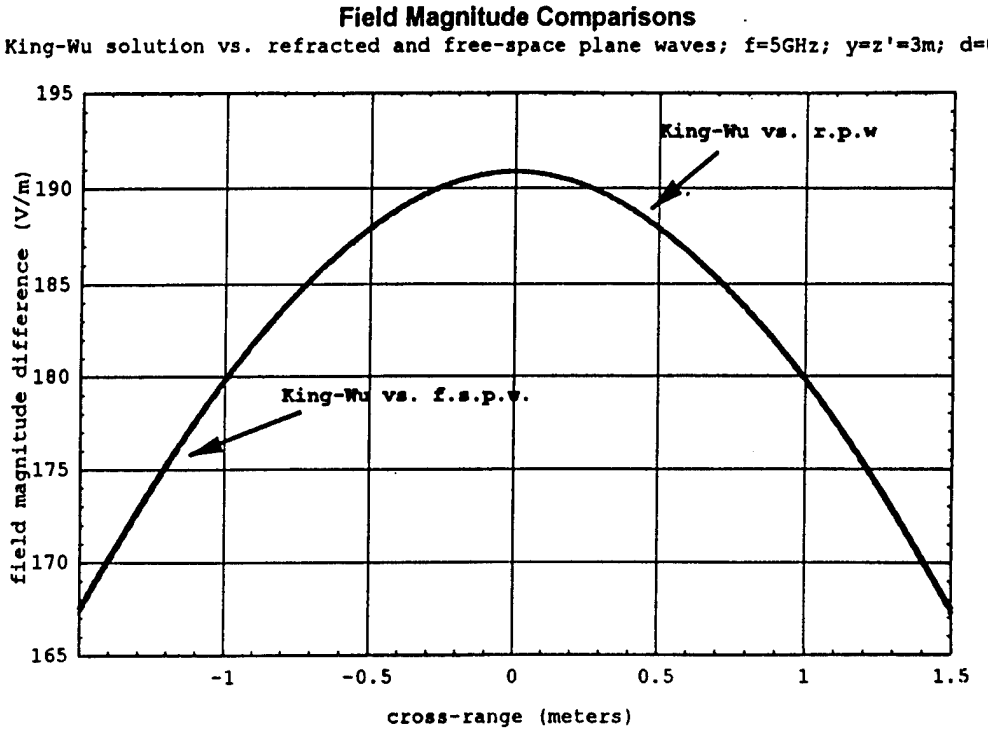

Figure 12. Field Magnitude Differences; $|z|$ = 3 m; f = 5 GHz

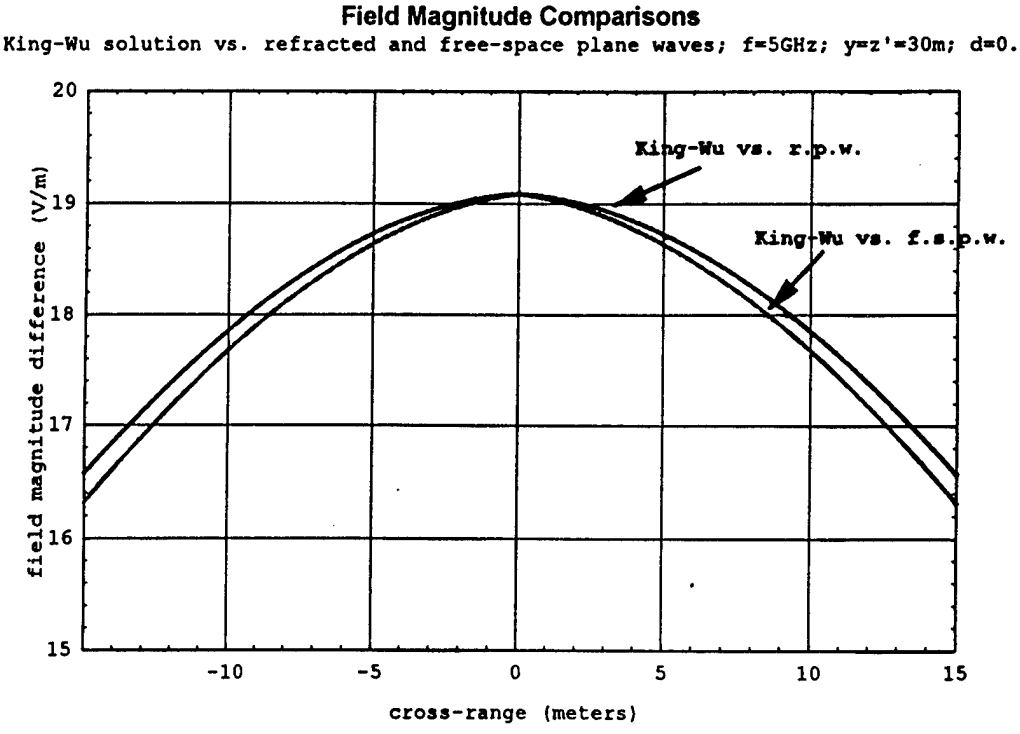

Figure 13. Field Magnitude Differences; $|z|$ = 30 m; f = 5 GHz

4. FINDINGS

The numerical results allow a comparative examination of the functions μ_i, Δ_i, and χ_j, where the phase and magnitude differences are interpreted as predictors, and the correlation functions as direct measures, of image reconstruction quality [9, 10, 11]. Inspection of the correlation functions in Figures 2 and 4 reveals that at frequencies of 600 MHz and 5 GHz, the 3 m altitude plane wave images are considerably degraded compared to the images correlated with the King-Wu solution. This is especially true in the case of images correlated with the free-space plane wave (FSPW) given in Eq. (6), whereas use of the refracted plane wave approximation (RPW) of Eq. (7) affords an obvious improvement over FSPW in terms of both central peak sharpness and relative height of the nearest sidelobes. However, Figures 3 and 5 reveal a significant difference in the distribution of power with respect to cross-range compared to the 3 m altitude results. In sharp contrast to the low altitude cases, at frequencies of 600 MHz and 5 GHz the 30 m altitude FSPW and RPW images nearly approximate the images correlated with the King-Wu solution. Compared to the King-Wu images, there is a loss in image intensity for both FSPW and RPW. However, at both frequencies the figure of merit afforded by the combination of central peak sharpness and relative height of nearest sidelobes is greatly improved for the plane wave approximations by receiving data at a higher altitude.

It has been known for many years that the phase history of a target is generally considerably more important than the spectral magnitude in the Fourier representation of signals used to reconstruct radar images [12]. This expectation is borne out by our results. Figures 6 through 9 show the comparative phase differences between the plane wave approximations and the King-Wu solution for the scenarios considered. What is of interest here is the dependence on cross-range of the phase differences, since a constant phase difference would be unimportant. The *slope* of the phase defect furnishes a relevant figure of merit in these graphs. For each of the four scenarios considered, the phase difference function predicts the trend indicated by the correlation functions. For the low altitude cases at both frequencies, the FSPW phase defects vary through as much as 2 radians, while the RPW phase defects are reduced at their maxima at each frequency by a factor of roughly one-third, consistent with a moderate improvement in image quality. However, when the receiver is elevated to 30 m a drastic reduction in the phase defect is observed. At 600 MHz

the maximum phase defect for both FSPW and RPW is reduced by a factor of roughly 60, and at 5 GHz the maximum phase defect for both plane waves is reduced by a factor of roughly 100, the greater improvement in the latter case resulting from the greater number of wavelengths separating receiver and source. The differences in field magnitude shown in Figures 10 through 13, although conforming to the trend established by the correlation functions, are as expected much poorer predictors of image quality than the phase difference functions.

5. CONCLUSIONS

In sum, we have shown explicitly that, when the receiving antenna is very close to the ground above a buried source, the use of plane wave approximations to correlate signals will lead to severely degraded images compared to images correlated with accurate analytical solutions to the Maxwell equations [Eqs. (2) through (4)]. In contrast, for many other cases of interest, when the receiving antenna is sufficently high (over 30 m altitude), the quality of images correlated with a plane wave approximation is quite good apart from some loss in image intensity.

REFERENCES

1. T. Ozdemir, S. Roy and R. Berkowitz, "Imaging of Shallow Subsurface Objects: An Experimental Investigation," *IEEE Trans. on Geoscience and Remote Sensing,* Vol. 30, No. 3, pp. 472–481, May 1992.

2. J.G. Proakis and D.G. Manolakis, in Chapter 6 of *Introduction to Digital Signal Processing,* Macmillan, New York, 1988.

3. T. Tamir, in Chapter 13 of *Electromagnetic Surface Modes,* edited by A.D. Boardman, Wiley, New York, 1982.

4. G. Gilbert, M. Braunstein and J. Ralston, work in progress.

5. R.W.P. King, M. Owens, and T.T. Wu, *Lateral Electromagnetic Waves,* Springer-Verlag, New York, 1992.

6. R.W.P. King, private communication to G. Gilbert, February 1994.

7. J.A. Stratton, *Electromagnetic Theory,* McGraw-Hill, New York, 1941.

8. N. Levanon, *Radar Principles,* Wiley, New York, 1988.

9. J.C. Curlander and R.N. McDonough, *Synthetic Aperture Radar: Systems and Signal Processing,* Wiley, New York, 1991.

10. D.L. Mensa, *High Resolution Radar Cross-Section Imaging,* Artech House, Norwood, 1991.

11. J.W. Goodman, *Introduction to Fourier Optics,* McGraw-Hill, New York, 1968.

12. A.V. Oppenheim and J.S. Lim, "The Importance of Phase in Signals," *Proc. IEEE,* Vol. 69, No. 5, pp. 529–551, May 1981.

APPENDIX

DERIVATION OF EQUATION FOR REFRACTED PLANE WAVE OFFSET DISTANCE

APPENDIX
DERIVATION OF EQUATION FOR REFRACTED PLANE WAVE OFFSET DISTANCE

If θ_1 and θ_2 are the formal transmission angles, then according to Snell's Law

$$k_1 \sin\theta_1 = k_2 \sin\theta_2 \quad . \tag{A1}$$

In the problems considered in this paper one has $k_1, \theta_1 \in \mathbf{C}$. However, to obtain the path length and transmission coefficient for refracted plane waves, we are interested instead in $\tilde{\theta}_1 \in \mathbf{R}$, the real, "geographical" angle which specifies through the offset distance a the location at which, in the geometrical optics limit, the refracted plane wave impinges on the air-ground interface. $\tilde{\theta}_1$ is determined by (cf. [7], p. 502)

$$\sin\tilde{\theta}_1 = \frac{k_2 \sin\theta_2}{\sqrt{q^2 + k_2^2 \sin^2\theta_2}} \quad , \tag{A2}$$

which is the "modified" Snell's Law appropriate to the case of plane wave incidence at a boundary separating lossy and lossless media. Here q is given by

$$q(a) = |u|\left[\mathrm{Re}k_1 \cdot \cos(\arg u) - \mathrm{Im}k_1 \cdot \sin(\arg u)\right] \quad , \tag{A3}$$

where u is a complex function of a (through its dependence on θ_2) given by

$$u = \sqrt{1 - \left(\alpha^2 - \beta^2 - 2\alpha\beta i\right) sin^2\,\theta_2} \quad , \tag{A4}$$

and

$$\alpha \equiv \frac{k_2 \mathrm{Re}k_1}{|k_1|^2} \quad , \tag{A5}$$

$$\beta \equiv \frac{k_2 \mathrm{Im}k_1}{|k_1|^2} \quad . \tag{A6}$$

Also, from Figure 1 we see that

$$\sin\tilde{\theta}_1 = \frac{a}{r} = \frac{a}{\left(a^2 + d^2\right)^{1/2}} \quad . \tag{A7}$$

We require that the constraints in Eqs. (A2) and (A7) both be satisfied. We solve the constraints by substituting for θ_2 from Eq. (10b), which leads to a condition where a satisfies the following transcendental equation

$$q^2(a)a^4 - 2\rho q^2(a)a^3 + \left[q^2(a)\left(\rho^2 + z^2\right) - k_2^2 d^2\right] a^2 + 2\rho k_2^2 d^2 a - k_2^2 d^2 \rho^2 = 0 \quad , \quad \text{(A8)}$$

which is the same as Eq. (11) in the text.

REPORT DOCUMENTATION PAGE

Form Approved
OMB No. 0704-0188

1. AGENCY USE ONLY *(Leave blank)*	2. REPORT DATE	3. REPORT TYPE AND DATES COVERED
	April 1994	Final—November 1993–April 1994

4. TITLE AND SUBTITLE
Characterizing and Correcting Media-Induced Focus Errors in Synthetic Aperture Radar Imagery

5. FUNDING NUMBERS
DASW01 94 C 0054
A-155

6. AUTHOR(S)
Gerald Gilbert, Matthew Braunstein, James Ralston

7. PERFORMING ORGANIZATION NAME(S) AND ADDRESS(ES)
Institute for Defense Analyses
1801 N. Beauregard St.
Alexandria, VA 22311-1772

8. PERFORMING ORGANIZATION REPORT NUMBER
IDA Paper P-2978

9. SPONSORING/MONITORING AGENCY NAME(S) AND ADDRESS(ES)
Information Systems Office
ARPA
3701 North Fairfax Drive
Arlington, VA 22203

10. SPONSORING/MONITORING AGENCY REPORT NUMBER

11. SUPPLEMENTARY NOTES

12a. DISTRIBUTION/AVAILABILITY STATEMENT
Approved for public release; distribution unlimited.

12b. DISTRIBUTION CODE

13. ABSTRACT ***(Maximum 180 words)***

Recently, considerable attention has been directed to the use of airborne synthetic-aperture radar (SAR) for detecting both large and small underground objects. The reconstruction of images of buried objects from SAR data, however, often relies on assumptions and algorithms developed in the context of free-space radar propagation. Although in some cases the implicit assumption of free-space propagation can lead to acceptable results, in other important cases it will result in severe degradation to images of underground objects. In this paper we investigate the conditions under which significant improvements to image quality result if proper account is taken of the detailed effects of the soil medium on radar wave propagation. These effects are analyzed both in terms of the refraction of plane waves and via reference to general analytic solutions to Maxwell's equations. Quantitative predictions of the improvement in buried-target image focusing are presented for some realistic data collection scenarios, corresponding to airborne and ground-based SAR or microwave holography.

14. SUBJECT TERMS	15. NUMBER OF PAGES
synthetic-aperture radar (SAR), ground-penetrating radar (GPR), lateral waves	29
	16. PRICE CODE

17. SECURITY CLASSIFICATION OF REPORT	18. SECURITY CLASSIFICATION OF THIS PAGE	19. SECURITY CLASSIFICATION OF ABSTRACT	20. LIMITATION OF ABSTRACT
UNCLASSIFIED	UNCLASSIFIED	UNCLASSIFIED	SAR